Downloaded from rsta.royalsocietypublishing.org

PHILOSOPHICAL TRANSACTIONS OF THE ROYAL SOCIETY A MATHEMATICAL, PHYSICAL & ENGINEERING SCIENCES

A Study of the Oxidation Mechanisms of Some Austenitic Stainless Steels in Carbon Dioxide at 1123K by means of Charged-Particle Nuclear Techniques. III

P. Skeldon, J. M. Calvert and D. G. Lees

Phil. Trans. R. Soc. Lond. A 1980 **296**, 567-580
doi: 10.1098/rsta.1980.0194

Email alerting service

Receive free email alerts when new articles cite this article - sign up in the box at the top right-hand corner of the article or click **here**

To subscribe to *Phil. Trans. R. Soc. Lond. A* go to: **http://rsta.royalsocietypublishing.org/subscriptions**

This journal is © 1980 The Royal Society

Downloaded from rsta.royalsocietypublishing.org

A STUDY OF THE OXIDATION MECHANISMS OF SOME AUSTENITIC STAINLESS STEELS IN CARBON DIOXIDE AT 1123K BY MEANS OF CHARGED-PARTICLE NUCLEAR TECHNIQUES. III

By P. SKELDON†, J. M. CALVERT‡ and D. G. LEES†

† *Metallurgy Department, Manchester University, Manchester, M13 9PL, U.K.*

‡ *Physics Department, Manchester University, Manchester, M13 9PL, U.K.*

(*Communicated by R. B. Nicholson, F.R.S. – Received* 10 *January* 1979)

[Plates 1–4]

CONTENTS

The oxidation behaviour in carbon dioxide at 1123 K and a pressure of approximately 0.1MPa of a 20 % (by mass) Cr, 25 % (by mass) Ni, Nb-stabilized steel strengthened with a dispersion of titanium nitride has been studied by using charged-particle nuclear techniques and conventional methods. The nuclear techniques were used to study the growth mechanism, thicknesses and surface composition of the oxide. The scales consisted of an outer spinel layer, a Cr_2O_3 layer and then a silicon-rich layer at the

The Royal Society is collaborating with JSTOR to digitize, preserve, and extend access to *Philosophical Transactions of the Royal Society of London. Series A, Mathematical and Physical Sciences.* www.jstor.org

Downloaded from rsta.royalsocietypublishing.org

oxide–metal interface. The growth mechanism of the oxide has been studied by using ^{18}O as a tracer; substantial solid-state diffusion of oxygen took place but indirect evidence indicates that some cation transport also occurred. The relative amounts of the two contributions are not known but the relative contribution from oxygen transport is greater than in the case of the steel without the titanium nitride dispersion. The oxide scales were poorly adherent and sometimes buckled. On two specimens there was evidence for gaseous transport through the scale.

The interpretation of the data from which ^{18}O concentration profiles are obtained is discussed in detail.

1. Introduction

In associated investigations (Skeldon *et al.* 1980 *a*, *b*, subsequently referred to as I and II) charged-particle nuclear techniques were used to study the oxide growth mechanisms when (*a*) a niobium-stabilized austenitic steel (the standard steel), and (*b*) the standard steel with ceria deposited on its surface, were heated in carbon dioxide at 1123 K and a pressure of approximately 0.1 MPa. The present paper reports the results of an investigation of the oxidation mechanism of an alloy formed by strengthening the standard steel with a dispersion of TiN. The oxidation conditions were the same as those stated above.

2. Previous work

The composition of this steel is given in table 1; it is very similar to that of the standard stainless steel except for the addition of titanium. The alloy is given a nitridation treatment to convert the titanium into a TiN dispersion, and then outgassed in pure hydrogen to remove most of the excess nitrogen. This treatment produces dendritic particles of TiN within the grains and small amounts of Cr_2N at the grain-boundaries. Details of the nitridation and outgassing treatments have been given by Evans *et al.* (1974).

The oxidation behaviour of this alloy in CO_2 has been studied by Evans *et al.* (1974, 1976, 1977). In the first two papers, the oxidation tests were performed at 1123 K either in CO_2 containing 1 % (by volume) CO and 1200 parts/10^6 (by volume) H_2O at 2.03 MPa pressure, or in CO_2 containing 2 parts/10^6 (by volume) H_2O at 0.03 MPa pressure; no significant difference could be detected between the two sets of data. In the third paper the oxidation tests were carried out in the temperature range 1023–1173 K in CO_2 containing 1–2 % (by volume) CO with small amounts of methane and water at 2, 0.1 or 0.03 MPa. After oxidation times of *ca.* 1000 h the oxide consisted principally of Cr_2O_3 which contained small amounts of Fe, Ni and Si, and an underlying silicon-rich layer. Some areas of the scale showed titanium segregation which seemed to be associated with pre-existing titanium-rich stringers within the metal; apart from these there was very little evidence of titanium-enrichment in the oxide. At mass-gains in the range of 0.02–0.07 mg/cm^2, transient increases in the oxidation rate were sometimes observed, which then decayed rapidly. Otherwise, the oxidation rate decreased monotonically. After oxidation times of *ca.* 6000 h, a more porous oxide, rich in Fe, Mn and Ni, was observed above the Cr_2O_3 layer. It is interesting to note that in a photomicrograph of the duplex scale (Evans *et al.* 1976) the outer surface of the outer layer and the inner surface of the inner layer are both irregular, while the boundary between the layers is relatively flat. This suggests that the inner layer (which is Cr_2O_3) grew by means of oxygen diffusion and that the outer layer grew by means of cation diffusion. The association of titanium in the Cr_2O_3 with pre-existing titanium-rich stringers in the alloy, referred to above, supports this suggestion as

Downloaded from rsta.royalsocietypublishing.org

to the growth mechanism of the Cr_2O_3. On the other hand, Evans *et al.* (1977) have stated that for oxidation times > 500 h in the temperature range 1073–1173 K, the growth rate of the Cr_2O_3 layer is the same as on the standard steel. This implies, as they point out, that the rate-controlling step is the same. They believe that this step is diffusion of chromium in Cr_2O_3 because on the Arrhenius plot the best-fit straight line fits reasonably well the data for pure chromium oxidation, and the activation energy agrees with that obtained by Hagel & Seybolt (1961) for diffusion of chromium in Cr_2O_3.

3. Experimental procedure

(*a*) *Sample preparation*

The specimens of the TiN dispersion-strengthened alloy were supplied by Berkeley Nuclear Laboratories in the nitrided and outgassed condition. The composition is given in table 1. The specimens were *ca.* 1 cm × 1 cm × 0.04 cm and were used in the as-received condition. Before oxidation they were washed in soap solution, degreased and weighed.

Table 1. Alloy composition (% by mass)

Fe	Cr	Ni	Mn	Si	Nb	Ti	C
bal.	20.0	25.7	0.6	0.84	0.2	2.0†	0.0

† The nominal Ti content for this alloy is 1.55 % by mass.

Table 2. Oxidation times (hours)

number	total	natural CO_2	$C^{18}O_2$
1	360	216.25	143.75
2	308.25	140.75	167.50
3	111.50	0.0	111.50
4	376.20	66.60	309.60
5	861.35	94.75	766.60
6	161.60	19.80	141.80
7	188.50	92.75	95.75
8	48.70	0.0	48.70

(*b*) *Oxidation of Samples*

Oxidation times are given in table 2. All samples were oxidized at 1123 K in static carbon dioxide at a pressure of approximately 0.1 MPa. The procedure was the same as that described in detail in I, with the initial oxidation carried out in natural carbon dioxide followed by oxidation in carbon dioxide enriched in ^{18}O. The specimens were held at temperature while the gas was changed, and at the end of the experiment were cooled to room temperature *in vacuo*. As noted in I, because of the changing isotopic composition of the gas during oxidation, the expression '100 % effective concentration of ^{18}O ions' is used to refer to the oxide formed on an alloy oxidized in isotopically enriched gas alone.

(*c*) *Charged-particle nuclear techniques*

The nuclear technique used in this investigation to determine the ^{18}O concentration profile has been discussed elsewhere (Calvert *et al.* 1974) and also briefly in I. The $^{18}O(p, \alpha)^{15}N$ reaction was used to determine the concentration of ^{18}O in the scale as a function of depth;

Downloaded from rsta.royalsocietypublishing.org

elastic scattering was used as in I for normalization, and for determining the scale thickness and the composition of the oxide at the oxide–gas interface. The principles underlying the use of elastic scattering measurements in this work are discussed briefly in I.

The oxides on the TiN dispersion-strengthened alloy tended to spall, thereby giving rise to the problem, discussed more fully in § 3*e* of I, of quantifying the nuclear results in a precise way. The oxides had a speckled appearance arising from many small areas of exposed alloy from which oxide had spalled. Allowances had to be made in the analysis for the fraction of total beam that was therefore incident on the exposed alloy rather than on oxide. This was done by comparison of the spectrum of protons elastically scattered from a spalled sample with the spectrum from a standard sample of those now being considered; it was possible to find a sufficiently large area of adherent scale on the TiN dispersion-strengthened specimen number 1 (see table 2) to give an elastic scattering spectrum for reference purposes. Examination of this region of the specimen by means of a scanning electron microscope confirmed that very little, if any, oxide had spalled from the sample in the area covered by the proton beam. When the size of the spalled area is known as a proportion of the total area covered by the proton beam, the correctly normalized α-yield can be calculated.

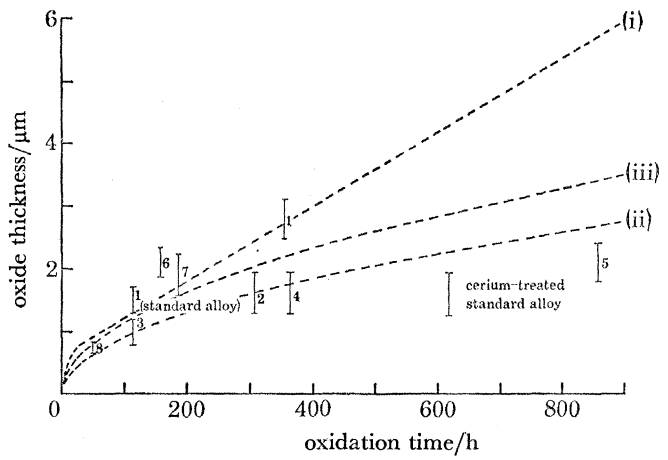

FIGURE 1. Oxide thickness (determined by elastic scattering) and oxidation time for the specimens used in this investigation. Unless otherwise stated the specimens are TiN dispersion-strengthened steel. The numbers refer to table 2. Curve (i) is taken from Francis & Whitlow (1965) for the standard steel. Curve (ii) is taken from Evans *et al.* (1976) for Cr_2O_3 formation on the TiN dispersion-strengthened steel. For curve (iii) see text. The results for the standard steel and the cerium-treated standard steel are taken from I and II respectively.

4. RESULTS

(*a*) *Oxidation kinetics*

Reliable mass-gain measurements were difficult to achieve because of the spalling of the scale referred to above. Therefore, scale thicknesses calculated from the results of elastic scattering experiments have been used to assess the oxidation rates. These scale thicknesses are plotted against oxidation time in figure 1. Curve (iii) on this figure has been calculated by using a value for the parabolic rate constant (k_p) equal to the average value of the parabolic rate constants of the samples of the dispersion-strengthened alloy calculated by assuming a parabolic relation between the scale thickness found from elastic scattering experiments and the oxidation time

Downloaded from rsta.royalsocietypublishing.org

($k_p = 3.73 \times 10^{-14}$ cm^2 s^{-1}). The spread in the data and the small number of samples prevent any accurate determination of a rate law. Curve (ii) shows the rate of thickening of the Cr_2O_3 layer on this alloy according to Evans *et al.* (1976) ($k_p = 2.32 \times 10^{-14}$ cm^2 s^{-1}). Curve (i) is that obtained by Francis & Whitlow (1965) for oxidation of the electropolished samples of the standard steel. The results from papers I and II are also plotted on this figure.

(*b*) *Appearance of oxidized samples*

Most samples had a speckled appearance which was caused by a fine mosaic of adherent dark grey oxide and metallic-coloured patches where the oxide had spalled. Usually approximately 50 % (by area) of the scale spalled, although there was a slight tendency for the amount of spalled oxide to increase with the time of oxidation. The spalled oxide was normally a fine dark grey powder, but sample 4 produced flakes of scale of area approximately 1 mm^2; the alloy surface had a dull metallic appearance.

TABLE 3. X-RAY DIFFRACTION RESULTS

oxide ... / sample	Cr_2O_3	spinel
1	w	s
3	s	s
5	w	s
6	s	m
8	s	s

s, strong; m, medium; w, weak.

TABLE 4. ENERGY DISPERSIVE X-RAY ANALYSIS RESULTS.

	Si	Ti	Cr	Mn	Fe	Ni
scale on sample 1	0.7	1.2	32.8	3.2	54.4	7.7
inner scale on sample 1	0.3	2.2	68.2	1.2	22.4	5.7
spalled area of sample 1	0.6	1.9	17.1	0.9	52.6	26.9
flake of scale from sample 4	0.2	1.6	79.9	12.2	6.1	0.0
scale on sample 6	1.7	0.4	80.1	15.3	2.5	0.0
spalled area of sample 6	5.9	1.9	15.9	0.0	53.1	23.2

(*c*) *Composition of scales*

The results of the X-ray diffraction measurements are given in table 3, and show that the oxides identified were Cr_2O_3 and spinel. (It should be noted that a small amount of Fe_2O_3 in the Cr_2O_3 would not be detected). For most samples, diffraction from the spinel produced the stronger diffraction peaks.

Energy dispersive X-ray analysis results are given in table 4. When the electron beam was incident on an area of sample 1 where the scale appeared to be fully adherent, the X-ray yield indicated the presence of a large amount of iron, a somewhat smaller amount of chromium and much smaller amounts of nickel, manganese, titanium and silicon. When the electron beam was directed upon oxide particles adherent to the alloy at locations where the bulk of the scale had spalled, the X-ray yield indicated that the major constituent was now chromium, the iron concentration was much lower, and the minor constituents were again nickel, manganese, titanium and silicon. Analysis of an area of this sample from which the oxide had completely spalled showed that the iron concentration was very much greater than that of the chromium, which suggests that as far as these two elements were concerned, the analyses of the oxides were

PHILOSOPHICAL TRANSACTIONS OF THE ROYAL SOCIETY A MATHEMATICAL, PHYSICAL & ENGINEERING SCIENCES
PHILOSOPHICAL TRANSACTIONS OF THE ROYAL SOCIETY A MATHEMATICAL, PHYSICAL & ENGINEERING SCIENCES

Downloaded from rsta.royalsocietypublishing.org

not seriously affected by signals coming from the substrate. The results indicate that the outer part of the scale was iron-rich and the inner part was chromium-rich. Analysis of adherent oxide on sample 6 showed, in contrast to the results for sample 1, that the major constituent was chromium, the manganese concentration was very much higher than in the underlying alloy and that the minor constituents were iron, silicon and titanium; no nickel was detected. For sample 4, a flake of oxide was analysed so that there was no possibility of interference from the underlying alloy. The results were quite similar to those for the scale on sample 6.

Analysis of an area of sample 6 from which the oxide had spalled showed greatly increased silicon and decreased chromium, nickel and manganese concentrations compared with the unoxidized alloy; in fact no manganese was detected, which correlates with the relatively high concentration of manganese found in the scale on this specimen. On the other hand, the area from sample 1, from which the oxide had spalled completely, showed a decrease in the silicon concentration and small increases in the manganese and nickel concentrations compared with the unoxidized alloy.

Elastic scattering experiments were carried out on adherent scale on sample 8 by using 4 MeV α-particles. This sample was oxidized for the shortest time but showed a strong X-ray diffraction signal from spinel (table 3). The elastic scattering measurements showed that chromium, manganese and possibly a small amount of iron were present in the surface of the scale.

From these results we believe that the scales consisted of a thin silicon-rich layer at the oxide–metal interface, that next to this there was a Cr_2O_3 layer and then a layer of spinel which contained chromium, manganese, iron and possibly a small amount of nickel. The titanium concentration in the flake of oxide from sample 4 was approximately the same as that in the unoxidized alloy. Silicon was detected in the flake of detached oxide, but we do not know whether it was distributed throughout the scale or whether it was present because some of the silicon-rich inner layer had become detached with the flake.

(*d*) *Scale Morphology* (figures 2–6, plates 1–4)

These pictures have been chosen to show the main features, which may be summarized as follows:

(i) the scales generally spalled in small patches;

(ii) the scales tended to be more adherent on specimens oxidized for shorter times;

(iii) much of the scale surface was often covered by whiskers of approximately 1 μm length;

(iv) the surfaces of the scales (which the evidence presented in § 4*c* suggests were spinel) were mostly fine-grained;

(v) on some of the samples the scales were buckled;

(vi) after long oxidation times, isolated crystals and crystalline excrescences appeared on the scale surface;

(vii) The surface of the alloy from which the scale had spalled was pock-marked on samples 8 and 3 (figures 2 and 3, plate 1), but rather angular on sample 1 (figure 5*b*, plate 3).

(*e*) *Measurement of oxide crystallite size*

An attempt was made to determine the size of the crystallites in the scales on sample 6 by using the broadening of X-ray diffraction peaks. The technique has been described by Peiser *et al.* (1955). A number of difficulties were encountered as discussed in II.

Downloaded from rsta.royalsocietypublishing.org

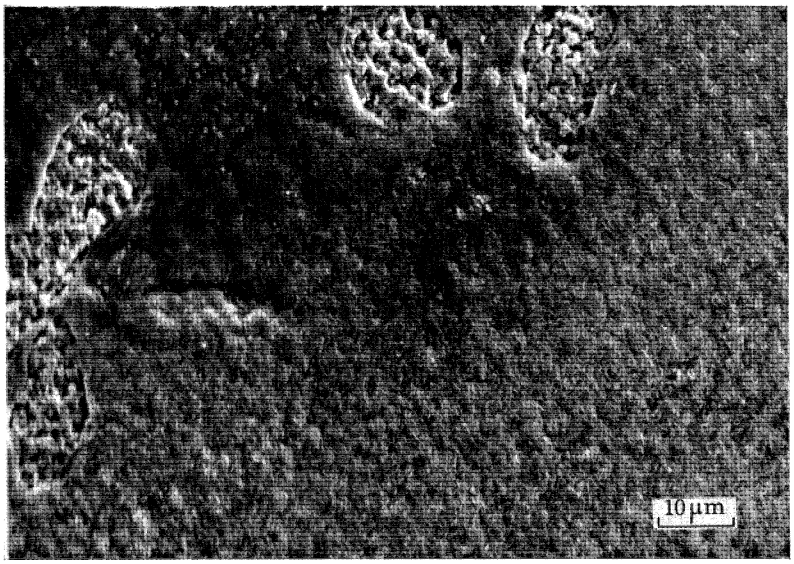

FIGURE 2. The surface of the scale on sample 8. Part of the scale has spalled. Electron acceleration energy = 30 keV.

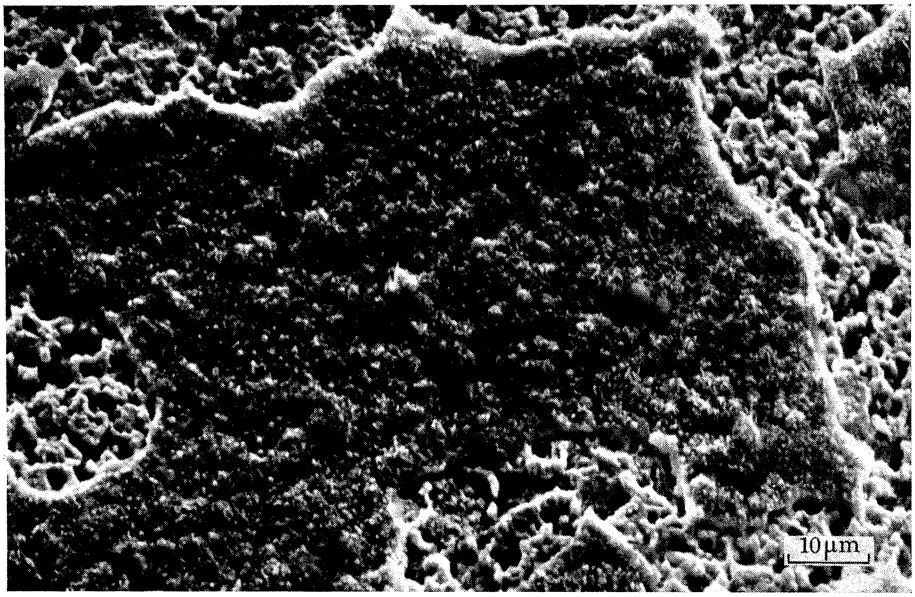

FIGURE 3. The surface of the scale on sample 3. Part of the scale has spalled. Whiskers can be seen on the surface of the scale at higher magnification. Electron acceleration energy = 25 keV.

(*Facing p.* 572)

PHILOSOPHICAL TRANSACTIONS OF THE ROYAL SOCIETY A MATHEMATICAL, PHYSICAL & ENGINEERING SCIENCES
PHILOSOPHICAL TRANSACTIONS OF THE ROYAL SOCIETY A MATHEMATICAL, PHYSICAL & ENGINEERING SCIENCES

Downloaded from rsta.royalsocietypublishing.org

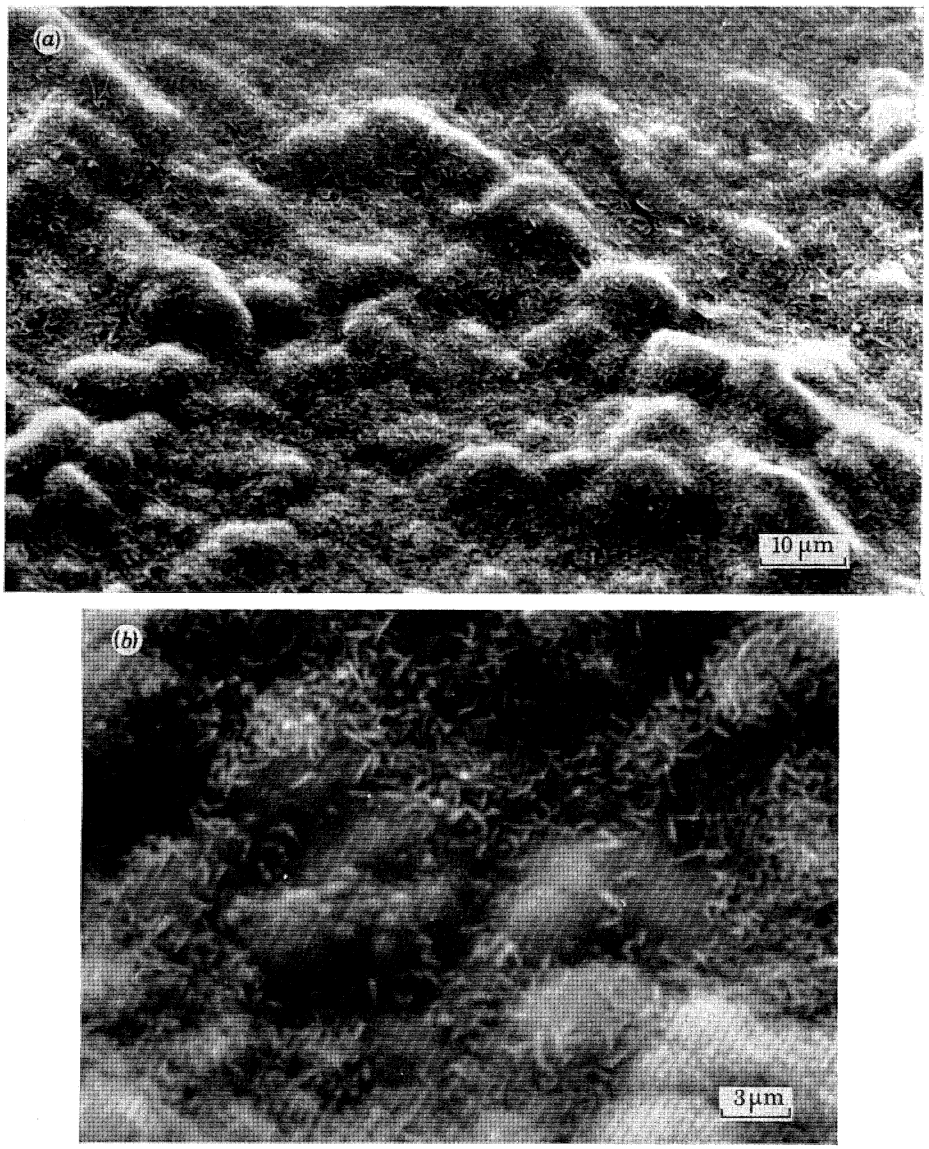

FIGURE 4 (*a*, *b*). The surface of the scale on sample 4. Note the beginning of buckling. In figure 4*b* there is a region that appears to have coarser grains. Electron acceleration energy = 30 keV.

PHILOSOPHICAL TRANSACTIONS OF THE ROYAL SOCIETY A MATHEMATICAL, PHYSICAL & ENGINEERING SCIENCES

PHILOSOPHICAL TRANSACTIONS OF THE ROYAL SOCIETY A MATHEMATICAL, PHYSICAL & ENGINEERING SCIENCES

Downloaded from rsta.royalsocietypublishing.org

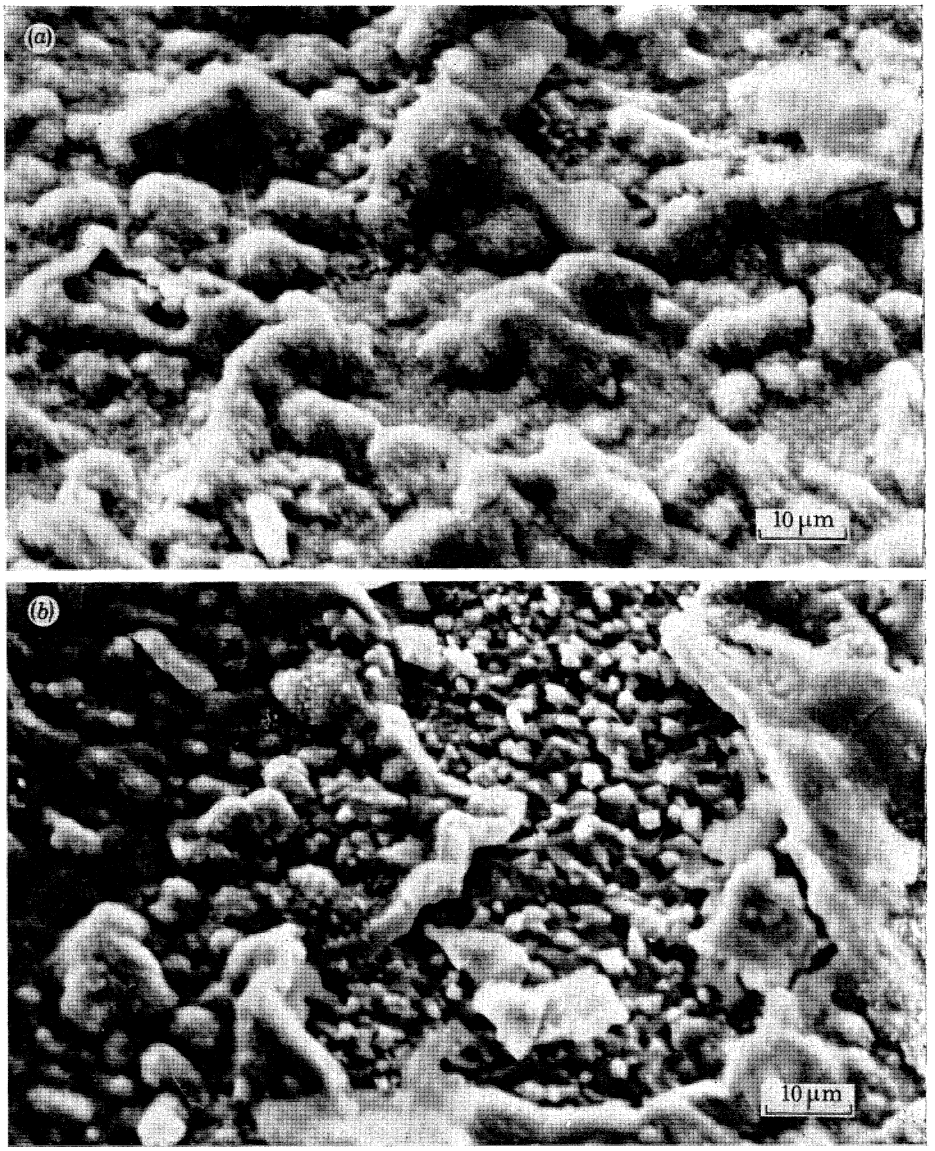

FIGURE 5 (*a*, *b*). The surface of the scale on sample 1. Note the broken part of the scale at the left of figure 5*a* which shows that the buckled regions are areas where the scale has lifted from the alloy. Figure 5*b* also shows that the scale has buckled and lifted from the surface. Electron acceleration energy = 30 keV.

PHILOSOPHICAL TRANSACTIONS OF THE ROYAL SOCIETY A MATHEMATICAL, PHYSICAL & ENGINEERING SCIENCES

PHILOSOPHICAL TRANSACTIONS OF THE ROYAL SOCIETY A MATHEMATICAL, PHYSICAL & ENGINEERING SCIENCES

Downloaded from rsta.royalsocietypublishing.org

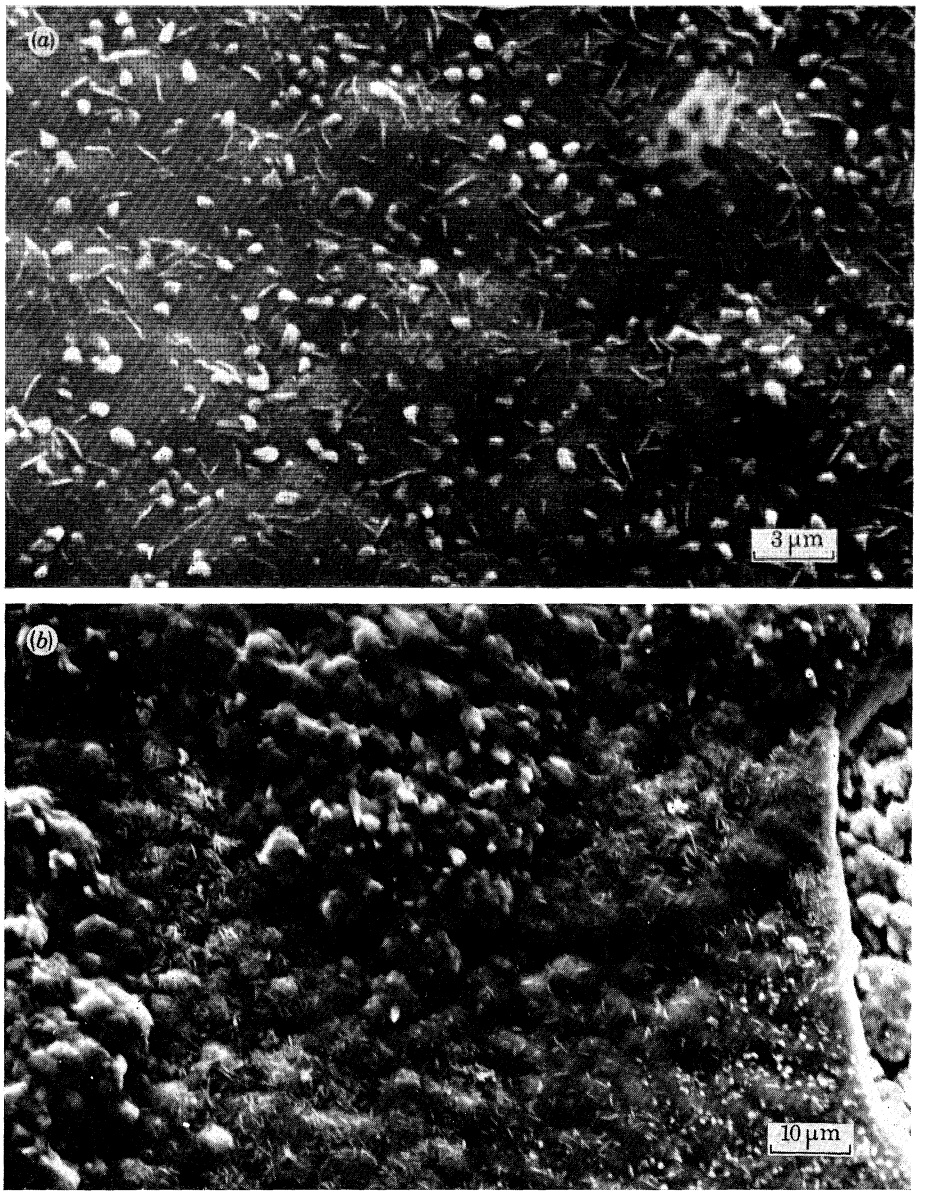

FIGURE 6 (*a*, *b*). The surface of the scale on sample 5. Whiskers are evident in figure 6*a* but not in such profusion as on some other samples. Figure 6*b* shows two regions. The scale at the top of the photograph has the appearance of an excrescence with coarse crystalline texture. The scale in the lower part of the picture is similar to that on samples oxidized for shorter times. Electron acceleration energy = 30 keV.

PHILOSOPHICAL TRANSACTIONS OF THE ROYAL SOCIETY A MATHEMATICAL, PHYSICAL & ENGINEERING SCIENCES

PHILOSOPHICAL TRANSACTIONS OF THE ROYAL SOCIETY A MATHEMATICAL, PHYSICAL & ENGINEERING SCIENCES

Downloaded from rsta.royalsocietypublishing.org

The few points that could be plotted and the errors associated with each point prevented an accurate measurement of the crystallite size, but the measurements indicate that the Cr_2O_3 layers on sample 6 had a crystallite size of *ca.* 0.1 μm.

(*f*) *The* ^{18}O *tracer distributions*

The significance of the graphs of α-yield against incident proton energy are discussed in detail in the appendix.

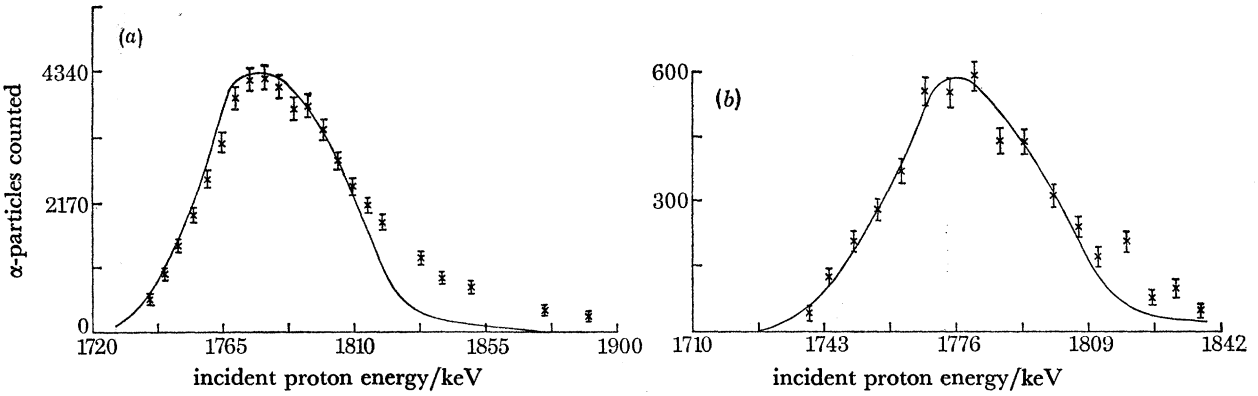

FIGURE 7*a*. A plot of α-particle yield against incident proton energy for sample 3. This specimen was only oxidized in $C^{18}O_2$. The continuous curve was computed for a step 0.95 μm thick.

FIGURE 7*b*. A plot of α-particle yield against incident proton energy for sample 8. This specimen was only oxidized in $C^{18}O_2$. The continous curve was computed for a step 0.7 μm thick.

Graphs of α-yield plotted against incident proton energy for two specimens of this alloy oxidized entirely in $C^{18}O_2$ are shown in figures 7*a*, *b* in which the continuous curve in each case has been computed for a step profile. Clearly this function does not give a perfect fit in either case. This is probably caused by the oxide thickness being non-uniform; variations of a few tenths of a micrometre would produce this effect. Samples 3 and 8 were used as reference specimens for measuring ^{18}O concentrations. The appropriate corrections, discussed in detail in § 3*e* of I, were applied in such a manner as to overestimate the concentration of ^{18}O in the surface of the scales of the sequentially oxidized specimens.

Figures 8–13 show the graphs of α-yield plotted against incident proton energy for specimens oxidized first in CO_2 containing natural oxygen and then in $C^{18}O_2$, together with the ^{18}O concentration profiles which have been deduced from these graphs. The fit to the experimental points was not sensitive to the type of function that was used, since equally good fits were obtained with exponential, and complementary error, functions. In all cases the latter function has been used, although even if this is the correct function the interpretation of the diffusion coefficient thus obtained must be treated with caution.

The concentration profiles fall into two groups:

Group 1 (figures 9–12)

(i) The concentration of ^{18}O falls continuously from the value at the scale surface in a manner that can be described by a complementary error function.

(ii) The concentration of ^{18}O at the scale surface is less than 100 %. As pointed out in § 3*e* of paper I, the resolution of the technique is such that if there were a thin (< 0.5 μm) surface layer with an effective ^{18}O concentration of 100 % it would not be recorded at this level.

(iii) There is no build-up of ^{18}O at the alloy–oxide interface.

PHILOSOPHICAL TRANSACTIONS OF THE ROYAL SOCIETY A MATHEMATICAL, PHYSICAL & ENGINEERING SCIENCES
PHILOSOPHICAL TRANSACTIONS OF THE ROYAL SOCIETY A MATHEMATICAL, PHYSICAL & ENGINEERING SCIENCES

Downloaded from rsta.royalsocietypublishing.org

Group 2 (figures 8 and 13)

(i) The concentration of ^{18}O at first falls continuously from the value at the scale surface in a manner that can be described by a complementary error function.

(ii) The concentration of ^{18}O at the scale surface is less than 100 %, though this statement should be qualified in the same way as the corresponding one for the group 1 specimens.

(iii) The concentration of ^{18}O at the alloy–oxide interface is greater than would be given by a continuation of the complementary error function.

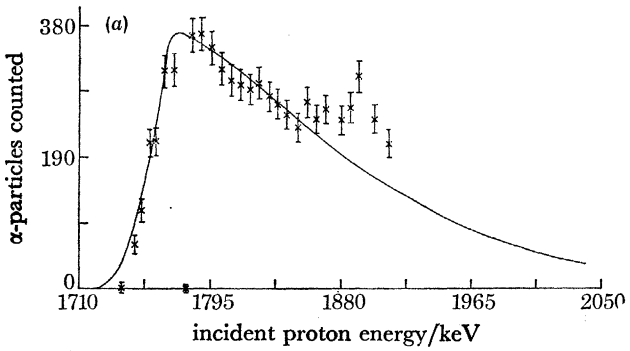

FIGURE 8*a*. A plot of α-particle yield against incident proton energy for sample 1. A value of 7.0×10^{-14} cm^2 s^{-1} was used in the complementary error function. (Continuous curve.)

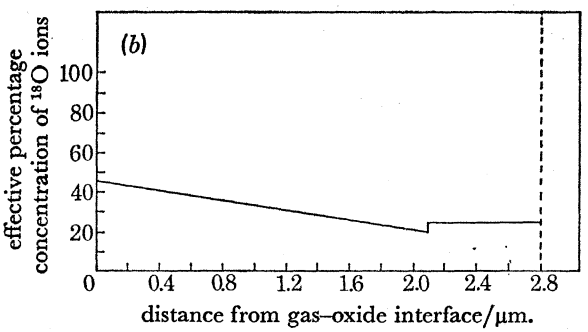

FIGURE 8*b*. The ^{18}O distribution deduced from figure 8*a*. This is a group 2 profile (see text). The shape of the profile near the alloy–oxide interface is very approximate because the effects of proton straggling reduced the resolution. The shape in this region should only be regarded as indicating a build-up of ^{18}O either at or near the alloy–oxide interface.

5. DISCUSSION

The evidence suggests that the scales on these specimens consisted of an outer spinel layer, inside this a layer of Cr_2O_3 and then a silicon-rich layer at the oxide–metal interface. In this respect they are similar to those on the standard steel (I) and, at least as far as the outer two layers are concerned, the cerium-treated standard steel (II).

The whole of the ^{18}O concentration profiles for specimens 2, 4, 5 and 6 (figures 9–12) and part of those for specimens 1 and 7 (figures 8 and 13), could be fitted with complementary error functions (with the reservations mentioned earlier). Thus in all cases substantial solid-state transport of oxygen occurred. The ^{18}O concentration profiles for samples 1 and 7 were higher than those predicted by the appropriate complementary error function near the oxide–metal interface. We believe that this was caused by gaseous transport which possibly occurred

Downloaded from rsta.royalsocietypublishing.org

during a transient increase in the oxidation rate, such as Evans *et al.* (1974) sometimes observed during the oxidation of this alloy. We have observed similar ^{18}O build-ups at the oxide–metal interface in the scales on pure chromium and some Fe–Cr alloys, and there, as here (figures 5*a*, *b*) the oxides were buckled (Barnes *et al.* 1973; Arjomand 1978). We believe that the oxide-buckling results from the formation of new oxide within the original oxide layer. If this is the case then some cation diffusion must have occurred. The presence of whiskers at the oxide–gas interface is probably further evidence for cation diffusion.

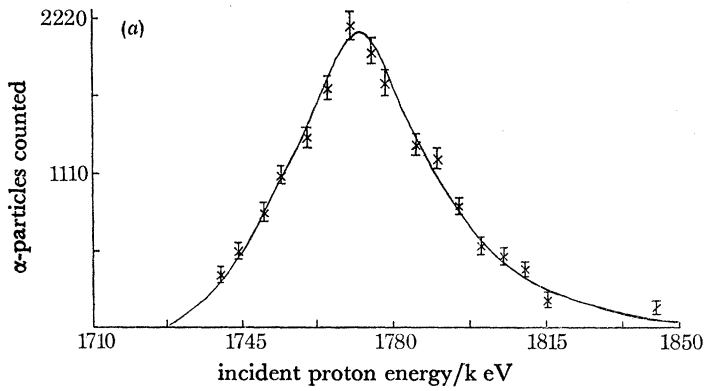

FIGURE 9*a*. A plot of α-particle yield against incident proton energy for sample 2. A value of 1.6×10^{-15} cm^2 s^{-1} was used in the complementary error function.

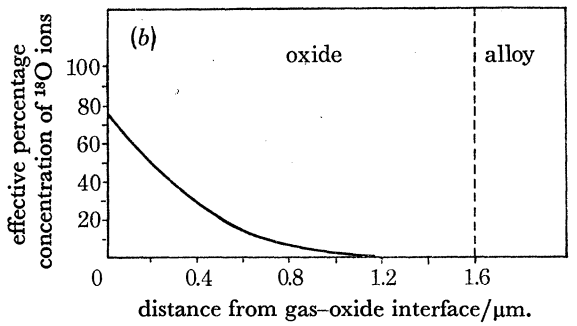

FIGURE 9*b*. The ^{18}O distribution deduced from figure 9*a*. This is a group 1 profile (see text).

When two processes operate in parallel, the faster one will be rate-controlling. Plainly the oxygen contribution to growth is substantial, but we do not know what its relative contribution is. For example, formation of an ^{18}O layer 0.3 μm thick at the oxide–gas interface would indicate an appreciable contribution from cation transport, because the total thickness of oxide formed during the $C^{18}O_2$ oxidations was probably 1 μm or less. Nevertheless a layer of this thickness would not have been detected during the present work for the reasons given in § 3*e* of I. However, it can be stated that the relative contribution from oxygen transport was appreciably greater than in the scale on the standard alloy. Evans *et al.* (1977) believe that, although oxygen transport is greater in the Cr_2O_3 layer on this alloy than in the Cr_2O_3 layer on the standard steel, the rate-controlling step is chromium diffusion through the oxide. The evidence that leads Evans *et al.* to this conclusion has been given in § 2 and may be summarized briefly as: (i) the Cr_2O_3 growth rates are the same for both alloys, (ii) the parabolic rate constants, when plotted on an Arrhenius graph, fall within the data for pure chromium, (iii) the activation

Downloaded from rsta.royalsocietypublishing.org

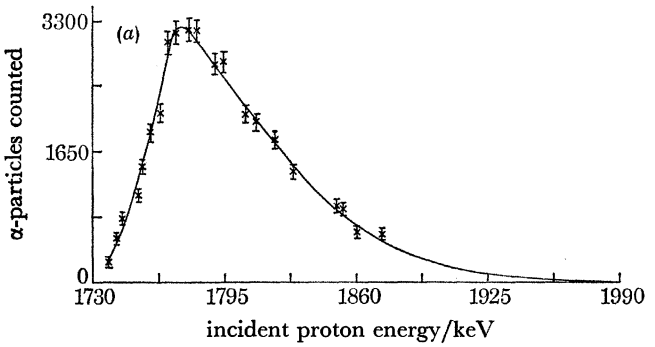

FIGURE 10*a*. A plot of α-particle yield against incident proton energy for a flake of oxide from sample 4. The proton beam was incident on the oxide–gas interface. A value of 6.5×10^{-15} cm^2 s^{-1} was used in the complementary error function. (Continuous curve.)

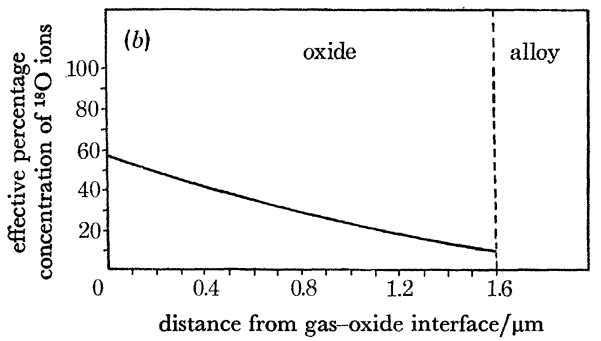

FIGURE 10*b*. The ^{18}O distribution deduced from figure 10*a*. This is a group 1 profile (see text).

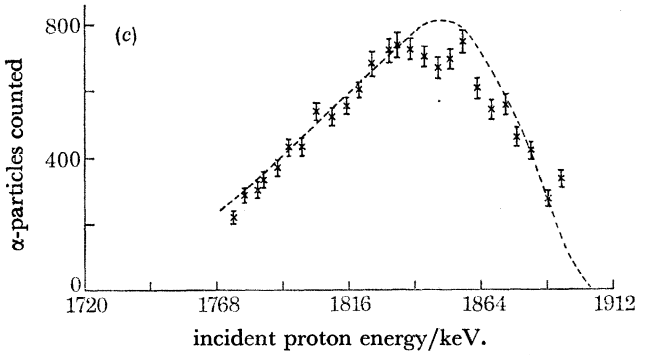

FIGURE 10*c*. A plot of α-particle yield against incident proton energy for a flake of oxide from sample 4 (a different flake from that referred to in figures 10*a*, *b*). In this case the proton beam was incident on the oxide–metal interface.

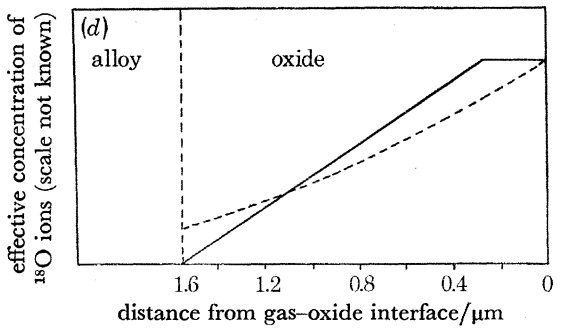

FIGURE 10*d*. The concentration profiles deduced from figures 10*a* (dashed line) and 10*c* (continuous line). In view of the resolution of the technique the two profiles should be regarded as similar.

Downloaded from rsta.royalsocietypublishing.org

energy is the same as that for diffusion of chromium in Cr_2O_3. As far as (i) is concerned, the oxide on several of our samples was buckled; under these circumstances the fact that different alloys oxidize at the same rate may not be significant. Furthermore, gaseous transport through the scales on samples 1 and 7 seems to have occurred, and this also casts doubt on the significance of kinetic data. The same comments then apply to the use of these data for Arrhenius plots and the calculation of activation energies. Therefore we feel that the deductions by Evans *et al.* may not be valid and that at this stage the rate-controlling step is not known.

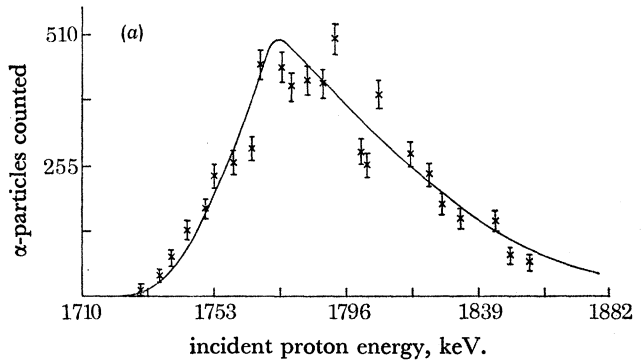

FIGURE 11*a*. A plot of α-particle yield against incident proton energy for sample 5. A value of 2.2×10^{-14} cm^2 s^{-1} was used in the complementary error function.

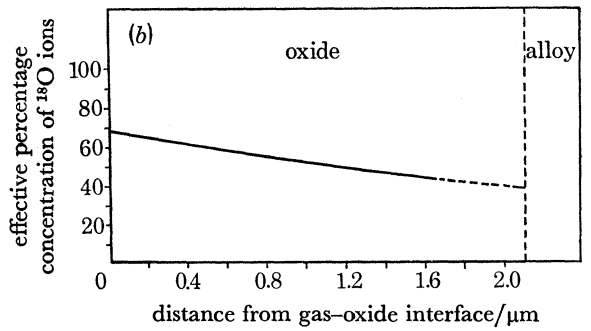

FIGURE 11*b*. The ^{18}O distribution deduced from figure 11*a*. This is a group 1 profile (see text). The shape of the profile beyond 1.6 μm is uncertain. Very little oxide remained on the alloy and the α-particle yield was low.

The low concentration of oxygen-18 indicates that the concentration profiles which we are studying arise from short-circuit diffusion; the contribution from bulk diffusion must extend such a short distance beneath the surface that it cannot be observed by our technique.

We attribute the difference between the growth-mechanisms of the oxides on the standard and the TiN dispersion-strengthened steels to the presence of titanium in the latter; 1.6% Ti was detected in a flake of the scale from the TiN dispersion-strengthened alloy (table 4). Cerium-treatment of the standard alloy also changed the oxide growth mechanism (II). The fact that scales on some specimens of the TiN dispersion-strengthened alloy buckled, whereas the scale on the cerium-treated standard alloy did not, may indicate that titanium is less efficient in blocking cation diffusion than is cerium, thus resulting in more oxide being formed within the oxide layer, or it could be that cerium improves the bonding at the oxide–metal interface better than does titanium, or both factors may be operating.

Downloaded from rsta.royalsocietypublishing.org

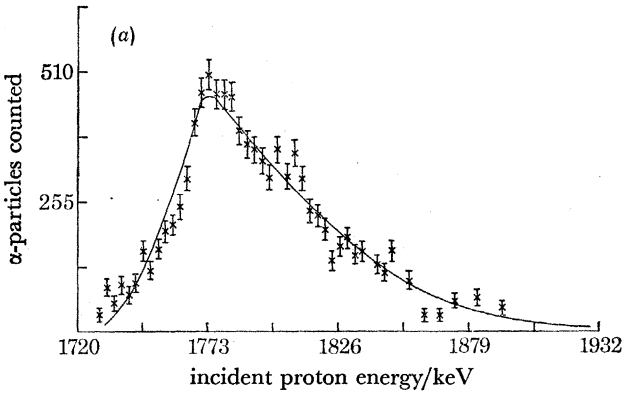

FIGURE 12*a*. A plot of α-particle yield against incident proton energy for sample 6. A value of 1.1×10^{-14} cm^2 s^{-1} was used in the complementary error function.

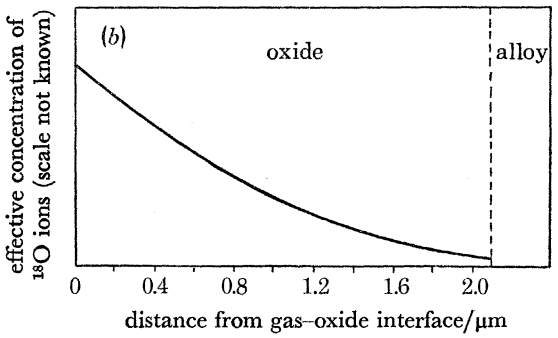

FIGURE 12*b*. The ^{18}O distribution deduced from figure 12*a*. This is a group 1 profile (see text).

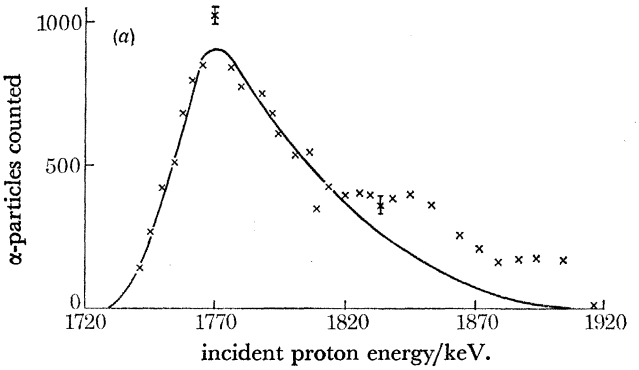

FIGURE 13*a*. A plot of α-particle yield against incident proton energy for sample 7. A value of 1.1×10^{-14} cm^2 s^{-1} was used in the complementary error function.

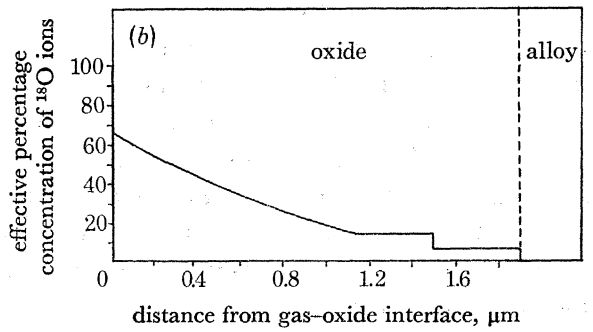

FIGURE 13*b*. The ^{18}O distribution deduced from figure 13*a*. This is a group 2 profile (see text).

Downloaded from rsta.royalsocietypublishing.org

6. Conclusions

The evidence suggests that the scale consists of an outer layer of spinel, inside that a layer of Cr_2O_3 and then a silicon-rich layer at the oxide–metal interface. The ^{18}O measurements show that the contribution of solid-state oxygen transport to the scale growth is substantial, but indirect evidence indicates that cation diffusion also occurs and the relative amounts of these two contributions are not known. The relative contribution from oxygen diffusion is appreciably greater than for the standard steel (I). We attribute this difference to the presence of titanium in the scale on the TiN dispersion-strengthened steel. Buckling of the scale was observed on several of the dispersion-strengthened specimens and in two cases there was evidence of gaseous transport through the scales.

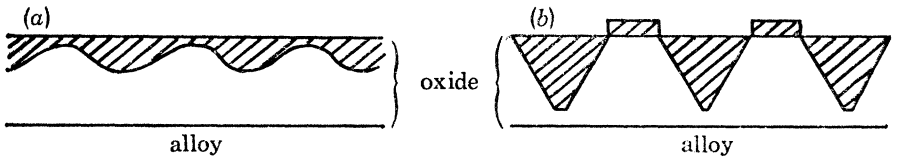

Figure 14 (*a*, *b*). Oxide morphologies which could produce ^{18}O distributions which would fit diffusion profiles although oxygen diffusion had not occurred. ▨, oxide formed in $C^{18}O_2$; □, oxide formed in $C^{16}O_2$.

Appendix. The significance of the graphs of α-yield against incident proton energy for the TiN dispersion-strengthened steel

The fact that a graph of α-yield against incident proton energy can be fitted with an error function does not necessarily mean that oxygen diffusion has occurred and therefore it is necessary to consider the significance of the α-yield plots. For example, a situation such as that depicted in figure 14*a*, where the roughness of the oxide changes between the beginning and end of the $C^{18}O_2$ oxidation, could produce an ^{18}O concentration profile that could be fitted with an error function even though no oxygen diffusion had occurred. However, in at least some of the samples the error function profile reached as far as the oxide–metal interface and the model proposed in figure 14*a* cannot account for this. In order to do so, it is necessary to postulate a situation such as that shown in figure 14*b*. In this case, at the end of the oxidation in $C^{16}O_2$, some regions of the oxide would have to be very thin, while the others would be much thicker. The thin regions would then have to grow appreciably during the $C^{18}O_2$ oxidation while the thick regions grew very little. (If the growth of the thick regions at this stage was $> 0.5\ \mu m$ – the approximate thickness corresponding to the width of the resonance in the $^{18}O(p, \alpha)^{15}N$ reaction – the effective ^{18}O concentration at the oxide–gas interface would be 100 %, whereas in every measurement it was substantially lower than this.) A wide range in the ratio of the oxidation times in $C^{16}O_2$ and $C^{18}O_2$ was used, and it does seem surprising that for the longer oxidation times in $C^{18}O_2$, ^{18}O distributions more closely approaching step-functions were not observed if substantial oxygen diffusion had not taken place. Furthermore, evidence on the morphology of the oxide after short oxidation times is provided by sample 8, the total oxidation time of which was shorter than the $C^{16}O_2$ oxidation times of all but one of the sequentially oxidized samples. The s.e.m. picture (figure 2) of the surface of the scale on this sample does not give any sign that the oxide thickness varies in the way suggested in figure 14*b*. Evidence is also provided by this sample on the matter of the effective ^{18}O concentration at the

Downloaded from rsta.royalsocietypublishing.org

oxide–gas interface of the sequentially oxidized samples because it was used as a reference sample. If the oxide layer on this sample varied in thickness in the manner required by the model, the α-yield would be less than that which would be obtained if the oxide thickness was uniform. This would then exaggerate the effective ^{18}O concentration of the specimen which was compared to it. Only if the ^{18}O layer on the sequentially oxidized specimen had a greater area which was < 0.5 μm thick than that of the reference specimen, would the effective ^{18}O concentration appear to be less than 100 %. Therefore, the fact that the effective ^{18}O concentration at the oxide–gas interface of this specimen (sample 7) is nevertheless much less than 100 % suggests that this is genuine and not produced by oxide roughness. On the other hand, the oxide scales on the standard steel, which grows primarily by cation diffusion as indicated by the marker-movement study by Tyzack *et al.* (1974), do have effective ^{18}O concentrations of 100 % at the oxide–gas interface (I). Furthermore, although ^{18}O is present at the oxide–metal interface in both samples of that steel, the curve of α-yield against incident proton energy for sample 1 of I (figure 6*a* of that paper) has a different shape from that given by a complementary error function, and most of the points fit well to the curve calculated by assuming a step-function. Yet it is interesting to note that the surface of the oxide on this sample (figure 3 of I) was rougher than that on most of the TiN dispersion-strengthened steel samples. We believe, therefore, that although the model postulated in figure 14*b* is not impossible, the most likely interpretation of the results for the TiN dispersion-strengthened steel is that substantial oxygen diffusion has occurred. This conclusion is supported by the indirect evidence discussed in § 1*c* and by the fact that the titanium concentration in a flake of detached scale was similar to that in the alloy.

We are grateful to the Science Research Council for financial support for one of us (P.S.) and for a research grant which assisted the work, and to the Berkeley Nuclear Laboratories of the Central Electricity Generating Board for financial support and the provision of material. We are also grateful to Dr H. E. Evans and Dr D. A. Hilton of Berkeley Nuclear Laboratories for helpful discussions.

References

Arjomand, M. 1978 M.Sc. thesis, Manchester Universty.
Barnes, D. G., Calvert, J. M., Hay, K. A. & Lees, D. G. 1973 *Phil. Mag.* **28**. 1303–1318.
Calvert, J. M., Derry, D. J. & Lees, D. G. 1974 *J. Phys.* D. **7**, 940–953.
Cox, B. & Roy, C. 1966 *Electrochem. Tech.* **4**, 121–127.
Evans, H. E., Hales, R., Hilton, D. A., Holm, R. A., Knowles, G. & Pearce, R. J. 1974 In *Corrosion of Steels in* CO_2 (ed. D. R. Holmes, R. B. Hill & L. M. Wyatt), pp. 369–380. British Nuclear Energy Society.
Evans, H. E., Hilton, D. A. & Holm, R. A. 1976 *Oxidat. Metals.* **10**, 149–161.
Evans, H. E., Hilton, D. A., Holm, R. A. & Webster, S. J. 1977 *Central Electricity Generating Board report* RD/B/N4062.
Francis, J. M. & Whitlow, W. H. 1965 *J. Iron Steel Inst.* **203**, 468–473.
Hagel, W. C. & Seybolt, A. U. 1961 *J. electrochem. Soc.* **108**, 1146–1152.
Peiser, H. S., Rooksby, H. P. & Wilson, A. J. C. 1955 *X-ray Diffraction by Polycrystalline Materials*. London: The Institute of Physics.
Skeldon, P., Calvert, J. M. & Lees, D. G. 1980*a* *Phil. Trans. R. Soc. Lond.* A **296**, 545–555.
Skeldon, P., Calvert, J. M. & Lees, D. G. 1980*b* *Phil. Trans. R. Soc. Lond.* A **296**, 557–565.

PHILOSOPHICAL TRANSACTIONS OF THE ROYAL SOCIETY A MATHEMATICAL, PHYSICAL & ENGINEERING SCIENCES
PHILOSOPHICAL TRANSACTIONS OF THE ROYAL SOCIETY A MATHEMATICAL, PHYSICAL & ENGINEERING SCIENCES

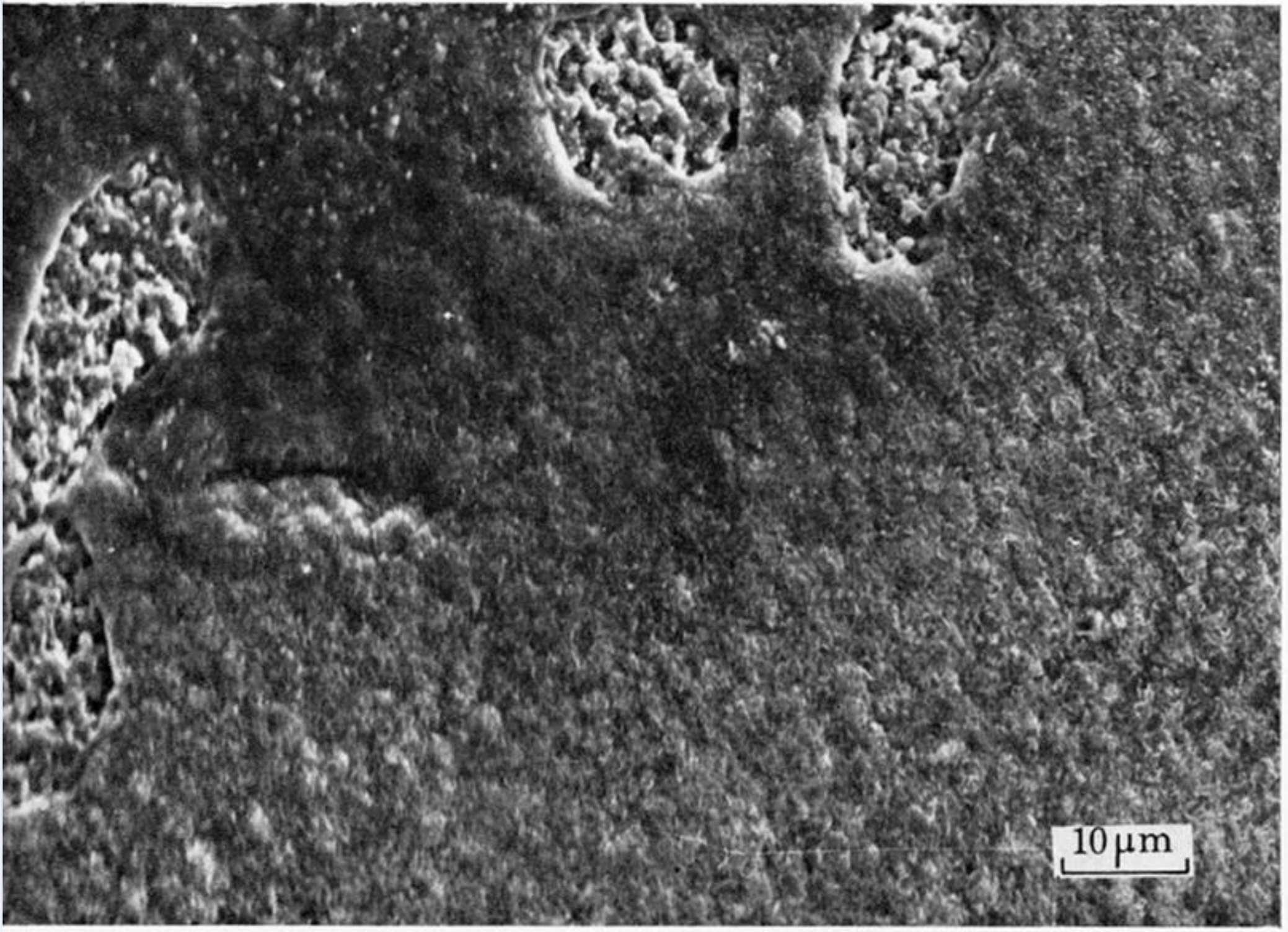

FIGURE 2. The surface of the scale on sample 8. Part of the scale has spalled. Electron acceleration energy = 30 keV.

PHILOSOPHICAL TRANSACTIONS OF THE ROYAL SOCIETY A MATHEMATICAL, PHYSICAL & ENGINEERING SCIENCES
PHILOSOPHICAL TRANSACTIONS OF THE ROYAL SOCIETY A MATHEMATICAL, PHYSICAL & ENGINEERING SCIENCES

PHILOSOPHICAL TRANSACTIONS OF THE ROYAL SOCIETY A MATHEMATICAL, PHYSICAL & ENGINEERING SCIENCES

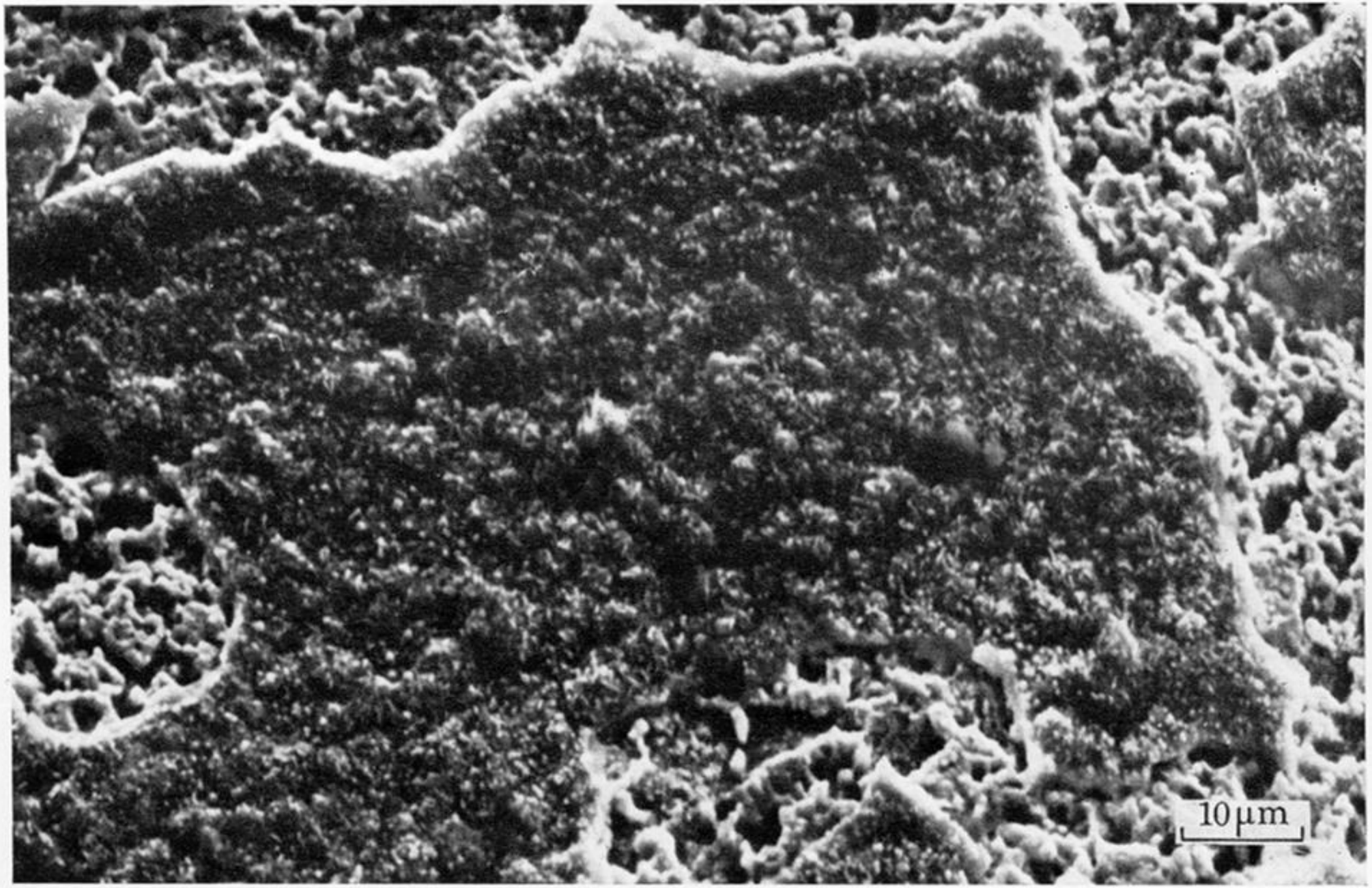

IGURE 3. The surface of the scale on sample 3. Part of the scale has spalled. Whiskers can be seen on the surface of the scale at higher magnification. Electron acceleration energy = 25 keV.

PHILOSOPHICAL TRANSACTIONS OF THE ROYAL SOCIETY A MATHEMATICAL, PHYSICAL & ENGINEERING SCIENCES

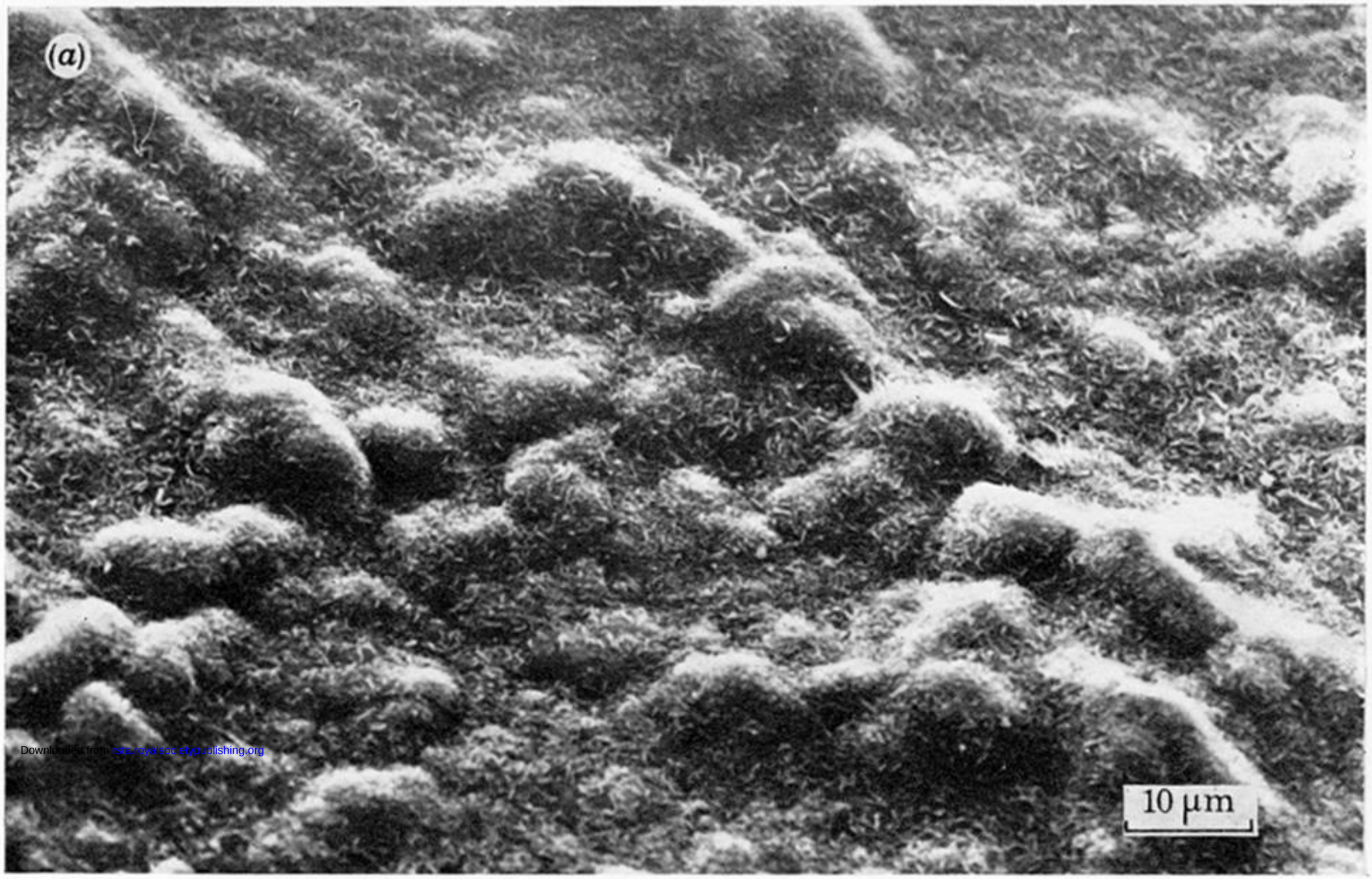

Downloaded from rsta.royalsocietypublishing.org

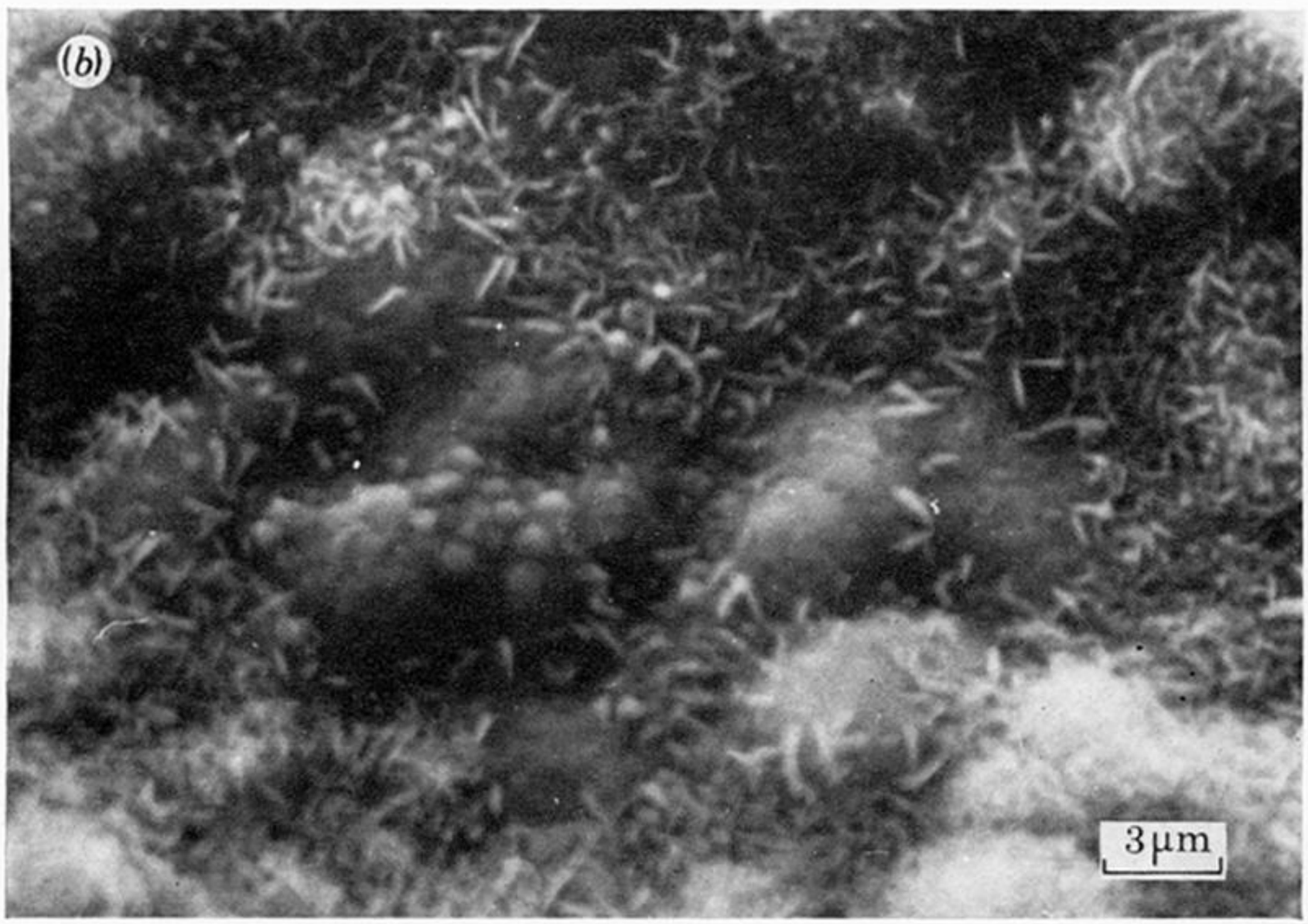

FIGURE 4 (*a*, *b*). The surface of the scale on sample 4. Note the beginning of buckling. In figure 4*b* there is a region that appears to have coarser grains. Electron acceleration energy = 30 keV.

PHILOSOPHICAL TRANSACTIONS OF THE ROYAL SOCIETY A MATHEMATICAL, PHYSICAL & ENGINEERING SCIENCES

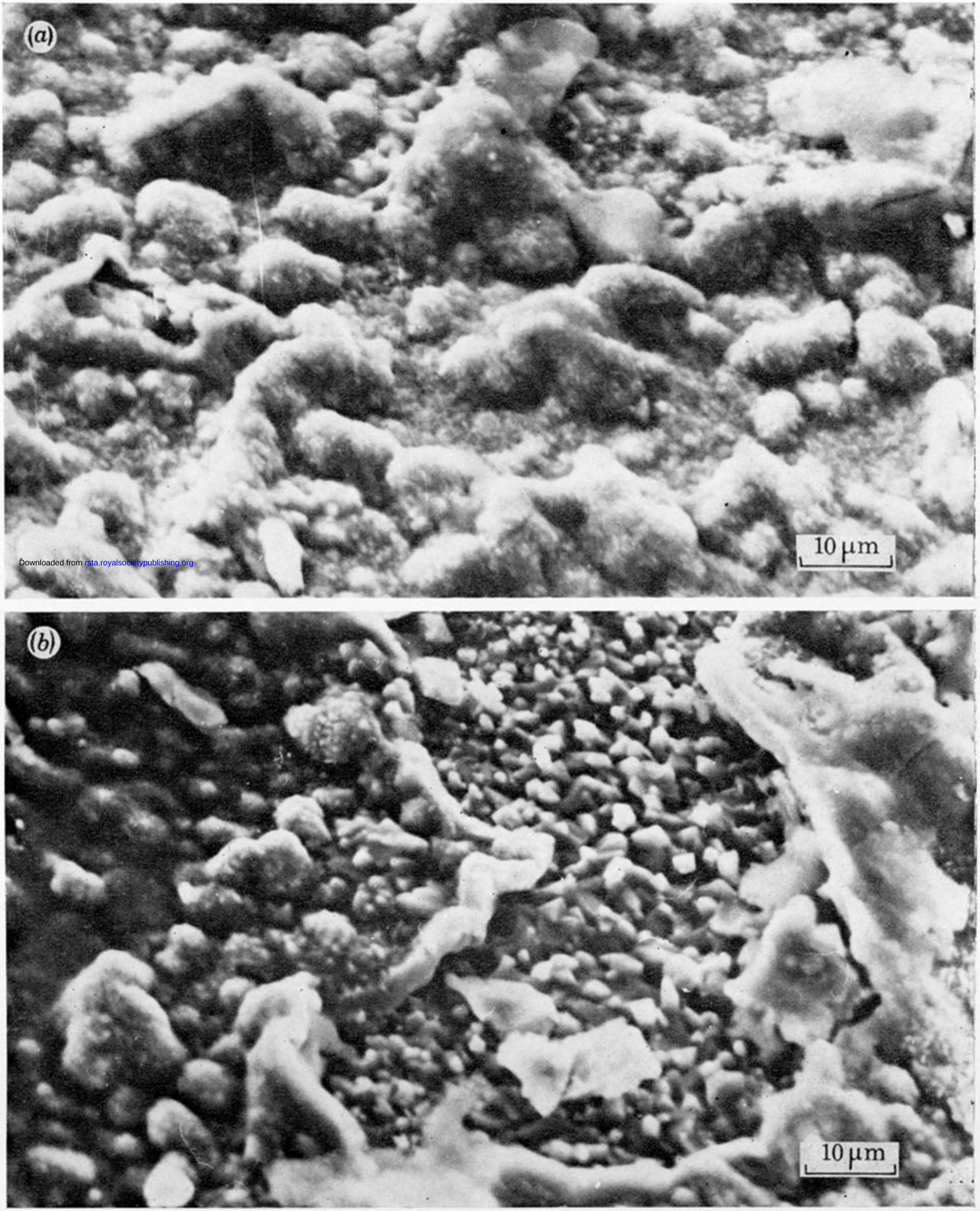

Downloaded from rsta.royalsocietypublishing.org

PHILOSOPHICAL TRANSACTIONS OF THE ROYAL SOCIETY A MATHEMATICAL, PHYSICAL & ENGINEERING SCIENCES

FIGURE 5 (*a*, *b*). The surface of the scale on sample 1. Note the broken part of the scale at the left of figure 5*a* which shows that the buckled regions are areas where the scale has lifted from the alloy. Figure 5*b* also shows that the scale has buckled and lifted from the surface. Electron acceleration energy = 30 keV.

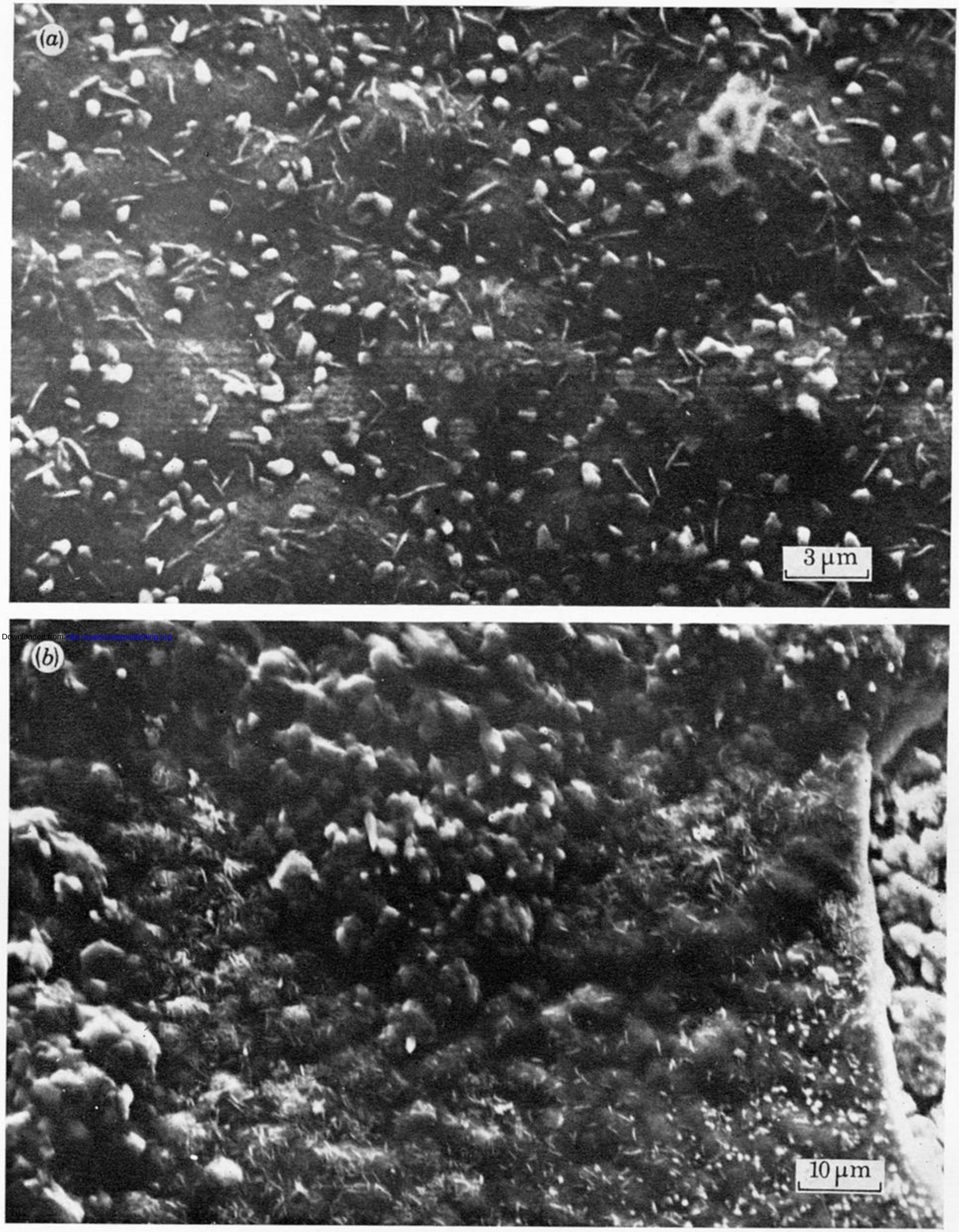

Downloaded from rsta.royalsocietypublishing.org

FIGURE 6 (*a*, *b*). The surface of the scale on sample 5. Whiskers are evident in figure 6*a* but not in such profusion as on some other samples. Figure 6*b* shows two regions. The scale at the top of the photograph has the appearance of an excrescence with coarse crystalline texture. The scale in the lower part of the picture is similar to that on samples oxidized for shorter times. Electron acceleration energy = 30 keV.

PHILOSOPHICAL TRANSACTIONS OF THE ROYAL SOCIETY A MATHEMATICAL, PHYSICAL & ENGINEERING SCIENCES